Unprecedented Catalytic Activity and Selectivity in Methanol Steam Reforming by Reactive Transformation of Intermetallic In-Pt Compounds

Nicolas Köwitsch[1], Lukas Thoni[2], Benjamin Klemmed[2], Albrecht Benad[2], Paul Paciok[3], Marc Heggen[3], Alexander Eychmüller[2], Marc Armbrüster[1] *

[1] *Faculty of Natural Sciences, Institute of Chemistry, Materials for Innovative Energy Concepts, Technische Universität Chemnitz, 09107 Chemnitz, Germany*

[2] *Physical Chemistry, Technische Universität Dresden, Bergstr. 66b, 01062 Dresden, Germany*

[3] *Ernst Ruska-Centrum, Forschungszentrum Jülich, 52425 Jülich, Germany*

* *marc.armbruester@chemie.tu-chemnitz.de*

Keywords

methanol steam reforming, intermetallic compounds, aerogel, HR-TEM, heterogeneous catalysis, $PtIn_2$, Pt_2In_3, Pt_3In_7, isotope labelling

Abstract

Hydrogen storage in form of small molecules and subsequent release is foreseen to play a fundamental role in future energy systems or carbon cycles. Methanol is an ideal hydrogen carrier due to the high H:C ratio, the lack of C-C bonds and being liquid at ambient conditions. Methanol steam reforming (MSR) is an advantageous reaction for the release of the chemically bound hydrogen. Pd- or Pt-based intermetallic compounds have shown to be CO_2-selective and long-term stable catalytic materials. However, intrinsic understanding of the underlying processes is still lacking. In this study we show, that the redox-activity in the In-Pt system can be steered by gas phase changes and leads to highly active catalytic materials at 300 °C (1500 mol(H_2)/(mol(Pt)×h)) with an excellent CO_2-selectivity of 99.5%, thus clearly outperforming previous materials. Reactive transformations between In_2Pt, In_3Pt_2 and In_2O_3 have been identified to cause the high selectivity. Redox-activity of intermetallic compounds as part of the catalytic cycle was previously unknown and adds understanding to the concept of different adsorption sites.

Introduction

Methanol steam reforming (MSR, eq. 1) is likely to play a fundamental role in future energy storage and distribution systems.[1–4] Catalytic materials, which are often derived from the

industrial methanol synthesis catalyst $Cu/ZnO/Al_2O_3$[5–10], must exhibit a high CO_2-selectivity by suppressing the concurring methanol decomposition (MD, eq. 2) and reverse water gas shift reaction (RWGS, eq. 3) for direct use of the product gases in proton exchange membrane fuel cells.[11]

$$CH_3OH + H_2O \rightleftharpoons 3\ H_2 + CO_2 \qquad (1)$$

$$CH_3OH \rightleftharpoons 2\ H_2 + CO \qquad (2)$$

$$CO_2 + H_2 \rightleftharpoons H_2O + CO \qquad (3)$$

Cu-based materials lack long-term stability and are pyrophoric, hindering practical application despite their good CO_2-selectivity of up to 99% at 300 °C.[12] *Iwasa et al.* described several Pt- or Pd-containing systems as well-performing MSR catalytic materials with pronounced stability during time on stream.[13–15] Formation of intermetallic compounds, e.g. ZnPd, InPd or In_2Pt, during operation has been identified to be of crucial importance for these noble-metal materials. *Tsai et al.* attributed the excellent catalytic performance of the intermetallic compound ZnPd to its electronic structure, being almost identical to elemental copper.[16] Pure ZnPd was proven to be CO_2 unselective and requires the presence of ZnO to exhibit a high CO_2-selectivity.[17–19] For several other Pd/metal oxide systems, formation of intermetallic compounds or oxidative decomposition of pre-formed intermetallic compounds under reaction conditions has been observed.[20] In addition to the mandatory teamwork between intermetallic compound and supporting metal oxide, an active redox-chemistry between two intermetallic compounds and a metal oxide was recently proven to be responsible for the very high CO_2-selectivity for $In\text{-}Pd/In_2O_3$.[21] This elucidates the need of understanding and controlling the redox-behavior of intermetallic compounds under reaction conditions.

Intermetallic compounds in the In-Pt system are known to catalyze MSR[13,22–24], the electrochemical oxygen reduction reaction[25], alcohol oxidation[26] and dehydrogenation of propane.[27,28] In MSR a high CO_2-selectivity of 98.3% is ascribed to the formation of In_2Pt[15] and the presence of partly reduced indium oxide.[29] According to recent findings in aerogel-supported intermetallic In-Pd compounds[21], an active redox-chemistry between two intermetallic compounds is necessary for high CO_2-selectivity. Here, the slight compositional changes of In_2Pt to In_3Pt_2 should hinder reactive sintering, allowing the creation of highly dispersed, nanoparticulate redox centers as catalytically active regions. Analogous to InPd and In_3Pd_2 a reactive transformation of In_2Pt to In_3Pt_2 or vice versa should generate redox centers.

At these centers, oxidic indium species will presumably participate in the catalytic cycle by acting as oxidizing agents for CO or reaction intermediates to form CO_2.

For this study, the as-prepared and pre-treated Pt/In_2O_3 aerogels were investigated regarding morphology by scanning and transmission electron microscopy (SEM, TEM), Pt-loading by inductively coupled plasma with optical emission spectroscopy (ICP-OES), specific surface area (nitrogen physisorption measurements), reduction behavior by thermogravimetry coupled with mass spectrometry (TG/MS) and crystalline phases by powder X-ray diffraction (XRD). The pre-treated material was subjected to MSR conditions with different reactant ratios and characterized after every test by XRD to correlate catalytic activity and selectivity with the present crystalline phases and potential redox-activity. High resolution transmission electron microscopy (HR-TEM) and high-resolution scanning transmission electron microscopy combined with energy-dispersive X-ray spectroscopy (STEM/EDX) were applied to samples after different applied MSR conditions to obtain nano-scale information about the influence of these conditions on the material, e.g. encapsulation effects, amorphization or compositional gradients inside the Pt-containing particles. ^{18}O-labeled MSR was conducted to identify the role of redox cycles during catalytic operation on the catalytic properties of the material.

Experimental

Catalyst preparation

$InCl_3$ (Alfa Aesar, 99.999%) was dissolved in ethanol (Berkel AHK, 99%, 1% petrol ether) to obtain a 0.25 M solution. To 10 mL of this solution 2.5 mL of water (Milli-Q) were added and stirred for 5 minutes. Subsequently, 5 mL of propylene oxide (Sigma Aldrich, 99%) were added to initiate gelation.[30] After stirring for 2 minutes, 0.889 mL of a 0.2 M ethanolic solution of $PtCl_4$ (Sigma Aldrich, 99.999%) were added during gelation of the oxidic network. After 0.5 minutes, 2 mL of a 0.053 M solution of $NaBH_4$ (Sigma Aldrich, 99.99%) in water were added to the mixture to reduce the metal salt and form metal nanoparticles, which are then incorporated into the oxidic gel matrix during the gelation process. After stirring for 5 minutes the stirrer was removed. Gelation of this solution occurred over 12 hours at ambient temperature. Afterwards, the solvent was exchanged firstly to pure ethanol and secondly to acetone (Honeywell, puriss.). For the solvent exchange, the gels were submerged in a fivefold excess of the new solvent and the solvent excess was removed after 12 h with a pipette. This procedure was repeated 6 times for each solvent. The obtained solvogel was transferred into extraction shells and put in an autoclave, where the solvent was exchanged to liquid CO_2 (Air Liquide, 99.7%) over 36 hours at 60 bar and 12 °C. Supercritical drying was conducted through heating to 37 °C and increasing the pressure to 85 bar and subsequent controlled pressure release to ambient conditions.

Characterization

Elemental composition was determined by ICP-OES (Varian Vista RL). The samples were dissolved in freshly prepared aqua regia (hydrochloric acid, 37 wt-%, nitric acid, 68 wt-%, VWR chemicals AnalaR NORMAPUR), diluted to 5 vol-% aqua regia with deionized water and measured in triplicate.

Microstructural analysis was conducted by SEM (Hitachi SU8020) and TEM (JEOL JEM 1400plus). For SEM measurements the samples were transferred onto a carbon pad and an acceleration voltage of 2 kV was utilized. For TEM measurements samples were transferred by drop casting onto Formvar coated TEM grids of an acetone dispersion prepared by ultra sonication. Image recording was done with an acceleration voltage of 120 kV. For the determination of the particle size all particles in a minimum of three areas of a prepared sample were measured. This resulted in more than 100 measurement points per sample.

For physisorption measurements (Nova 3000e) the samples were degassed for 3 hours at 110 °C and subsequently measured at 77 K with nitrogen (Air Liquide, 99.999%) as adsorbent.

TG/MS (Netzsch STA 449 F3 Jupiter®, Pfeiffer Omnistar) measurements were conducted with 66 vol-% filled Al_2O_3 crucibles, corresponding to 10 – 20 mg. The samples were calcined in 20% O_2/He (Air Liquide, 99.999%) to analyze the amount and kind of adsorbents and residues from synthesis. Subsequently, the system was flushed with helium and the samples were reduced in 5% H_2/He (Air Liquide, 99.999%). By mass flow controllers (Bronkhorst EL-FLOW®), the gas flow was set to 40 mL/min. Background correction was conducted by subtraction of blank measurements. The ion current for m/z = 18 and m/z = 44 signals was used as indicator for H_2O and CO_2, respectively.

Phase analysis of crystalline phases was conducted for the as-prepared samples, after partial reduction and catalysis by XRD (STOE *Stadi P*, Cu $K\alpha_1$ radiation $\lambda = 1.54060$ Å, Ge(111) monochromator).

For HR-TEM (Fei Titan 80-300 TEM[31]) and HR-STEM-EDX (Fei Titan 80-200 ChemiSTEM[32]) analysis, catalytic tests were stopped at different temperature and time-on-stream for *ex situ* analysis.

Catalytic Testing

Catalytic tests were carried out in a fixed-bed reactor system (PID Eng&Tech, Microactivity Reference) connected to a MicroGC (Varian CP 4900, equipped with a 10 m back-flushed M5A column, a 20 m back-flushed M5A column and a 10 m PPU column, Agilent Technologies) for the simultaneous analysis of H_2 (10 m M5A column), CO (20 m M5A column) and CO_2 (PPU column). The as-prepared Pt/In_2O_3 aerogel was mixed with 200 mg catalytically inert graphite (ChemPur, < 100 µm, 99.9%) as dilutant and placed in the reactor tube (stainless steel coated with SiO_2, inner diameter 7.9 mm) on top of a quartz glass fleece. The material was pre-treated *in situ* according to the TG/MS results. For the catalytic tests, a mixture of 10% He/N_2 (45 mL/min, Air Liquide, 99.999%) was used as carrier gas, which was mixed with the 1:1 H_2O/CH_3OH vapor (0.01 mL/min $H_2O_{(l)}$, 0.0225 mL/min $CH_3OH_{(l)}$, Fisher Scientific, HPLC grade). Unreacted reactants were condensed in a cooling trap and the gas stream was further dried by a Nafion® membrane with a counter flow of N_2 (100 mL/min) after the reactor. The dry gas stream was then analyzed by online gas chromatography to determine the activity according to equation 4 and the CO_2-selectivity according to equation 5.

$$a = \frac{n(H_2)}{n(Pt)*h} \qquad (4)$$

$$S_{CO_2} = \frac{c_{CO_2}}{c_{CO}+c_{CO_2}+c_{CH_4}} \qquad (5)$$

The apparent activation energies were derived according to the Arrhenius equation from the slope of the plot of the natural logarithm of the conversion *X* against the reciprocal temperature.

For the investigation of the influence of the oxidation potential of the applied reactant stream on the catalytic performance, the $H_2O_{(l)}$ or $CH_3OH_{(l)}$ feed was increased to 0.02 or 0.045 mL/min, respectively

^{18}O-labeled MSR (water-^{18}O 99 at-%, methanol-^{18}O 95 at-%, Sigma Aldrich) was conducted at 300 °C with the same reactor setup. For the analysis of the gas phase, a mass spectrometer (Pfeiffer Omnistar) was connected to the system between reactor outlet and cooling trap. Reactant and product ion masses were recorded for ^{16}O, ^{18}O and mixed isotope compositions with a response time of three seconds. Before switching between different reactant compositions, the reactor was thoroughly purged with inert gas at 300 °C, to ensure the removal of remaining reactants with different oxygen isotopes and adsorbed species. Complete purging was ensured by reducing the MS-signals to the initial baseline of the inert gas. Switching between bypass line and reactor line during the purging process was also utilized to ensure, that upon switching between the gas lines no remaining reactants accumulate in the gas phase of the closed of part. Reaching of the baseline of the MS-signals with no signal rise upon lien switching proved the absence of remaining reactants in the reactor system. The whole purging process was conducted for more than 1 h before injection of the new reactants. The catalytic material was pre-run at 350 °C for 1 h to bring the material in the active state and for 2 h at 300 °C to limit the on-stream activation during the experiment.

Results and Discussion

SEM and TEM analysis of the as-prepared aerogel with 10.0(2) wt-% Pt loading (ICP/OES), revealed an open porous network structure (Figure S1) with finely dispersed Pt-particles (1.9 ± 0.5 nm) on a support structure, consisting of particles interconnected by fine threads (Figure S2). The material was X-ray amorphous (Figure S3), hence requiring a thermal treatment to transfer the as-prepared material into defined In-Pt intermetallic compounds supported on an In_2O_3-aerogel to derive reliable structure-property relationships. TG/MS analysis (Figure 1a) revealed a two-step mass loss of 20.7(5) wt-% during calcination in synthetic air. This is caused by the removal of adsorbed water and organic residues according to the detection water- and CO_2-ascribed signals in the MS. Subsequent reduction in 5% H_2 revealed a partial reduction step (**A**) accompanied by maxima in the m/z = 18 and m/z = 44 signals at 236 °C with a mass loss of 1.9(5) wt-%. This is close to the calculated 2.1 wt-% loss for the formation of In_3Pt_2. At 350 °C the reduction of the supporting In_2O_3 (**B**) begins, leading to a total mass loss of 15.8(5) wt-% at 600 °C (calculated 12.9 wt-%). The slightly higher mass loss can be explained by remaining residues after calcination, which are removed during reduction. XRD analysis of materials obtained after reduction at 240 °C, 300 °C and 340 °C for 1 h (Figure 1b) revealed the presence of different In-rich intermetallic compounds in dependence of the reduction temperature. At 240 °C a mixture of In_2Pt and In_3Pt_2 is obtained and at 340 °C the formation of In_7Pt_3 besides In_2Pt is identified. Thus, it can be concluded that different In-Pt intermetallic compounds are accessible by small temperature changes, which might also occur under reaction conditions. At 300 °C single-phase In_2Pt on In_2O_3 is seemingly obtained since the main reflection for the intermetallic compounds at 40° matches the In_2Pt reference and has a symmetric shape. No reflections for other intermetallic compounds are identified in this diffraction pattern. Thus, it can be concluded that other intermetallic compounds are not present or in quantities below the detection limit of XRD. Consequentially, 300 °C was chosen as pre-reduction temperature for the catalytic testing, since mixtures of different intermetallic compounds on the pre-treated material would lead to a mixture of the respective catalytic properties of the compounds and hinder the detection of reactive transformations of intermetallic compounds.

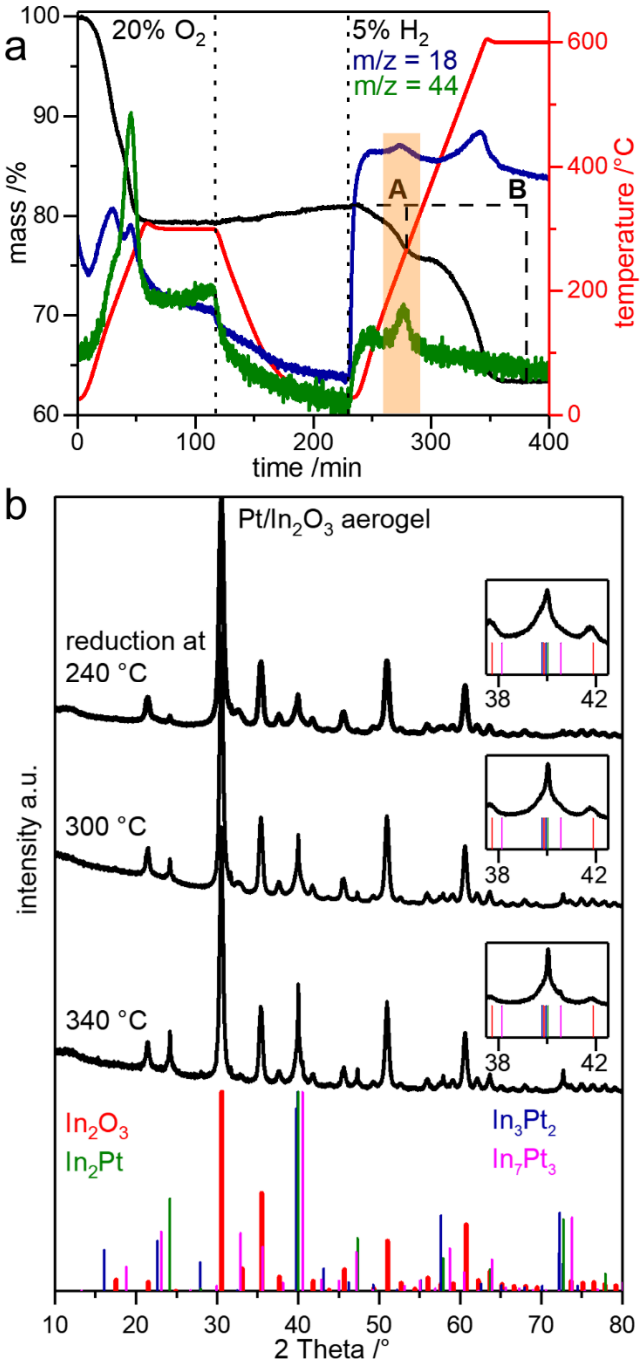

Figure 1: a) TG/MS measurement of the as-prepared Pt/In_2O_3 aerogel with the ion current for m/z = 18 and m/z = 44 as indicators for H_2O and CO_2, respectively. The orange inlay represents the temperature range of the partial reduction step. b) XRD patterns obtained after calcination and subsequent partial reduction at different temperatures along with the calculated patterns for In_2O_3[33], In_2Pt[34], In_3Pt_2[34] and In_7Pt_3.[35]

After pre-treatment a network structure with increased particle size can be identified by SEM (Figure S4). TEM analysis reveals the formation of cube-shaped particles out of the spider web analogue structure (Figure S5). This results in the decrease of the specific surface area from 145 m²/g to 47 m²/g. The particle size of Pt-containing particles increased slightly to 4.1 ± 1.1 nm, which is expectable based on thermal ripening and volume increase due to indium

incorporation. Pt-containing particles without an oxidic shell on the surface can be identified by HR-TEM on the crystalline support (Figure 2a). HR-STEM analysis (Figure 2b) together with EDX analysis (Figure 2c) revealed a homogenous elemental composition of the well-dispersed Pt-containing particles.

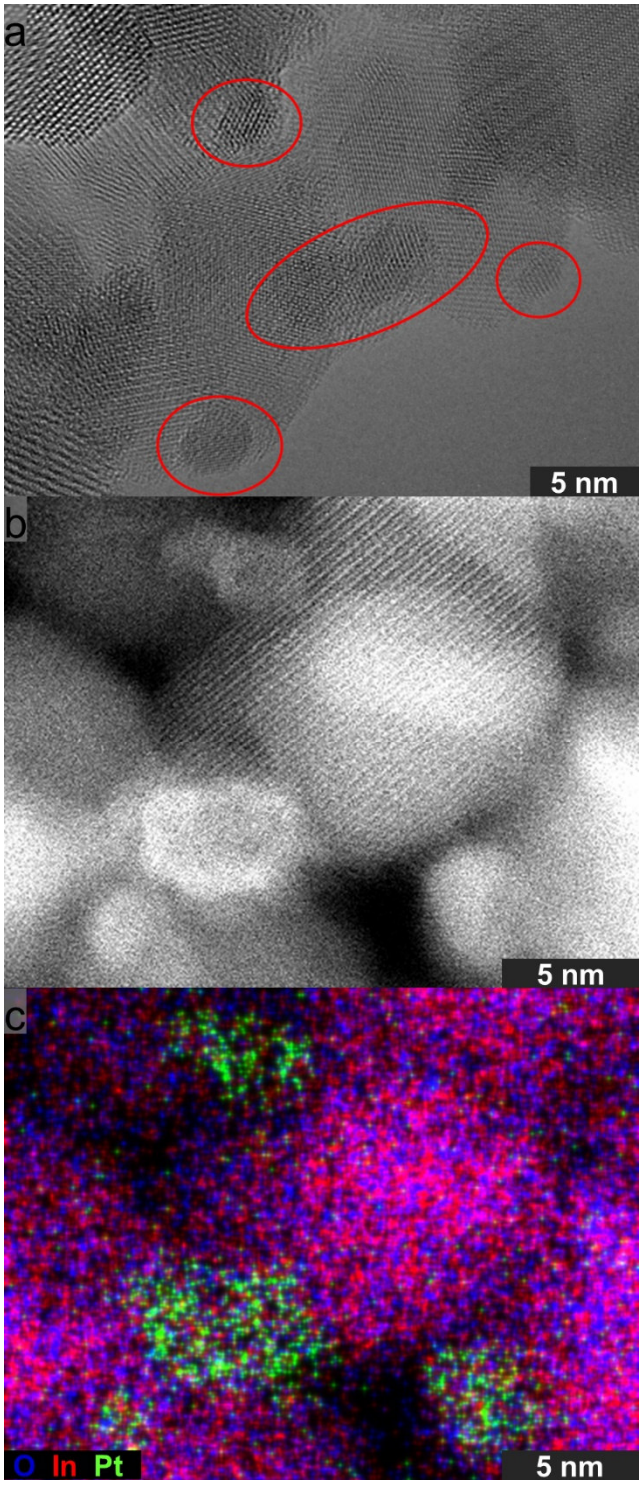

Figure 2: a) HR-TEM micrograph of the pre-treated material after partial reduction at 300 °C. The red ellipses emphasize Pt-containing particles in sub 10 nm domains. b) HR-STEM micrograph of the pre-treated material. Pt-containing particles can be identified by the higher contrast. c) Corresponding EDX mapping to the HR-STEM micrograph.

Catalytic testing in the temperature range of 200 – 300 °C (Figure 3a) revealed a high activity of 800 mol(H_2)/(mol(Pt)×h) along with an unprecedented CO_2-selectivity of 99.5% at 300 °C. During 20 h of isothermal testing at 300 °C, a continuous activation occurred. The activity increased from 545 mol(H_2)/(mol(Pt)×h) to 800 mol(H_2)/(mol(Pt)×h) during this period. An apparent activation energy E_A = 119(2) kJ/mol was derived by an Arrhenius-plot for the temperature range 200 – 300 °C (Figure S6). Isothermal testing at 300 °C (Figure S7) revealed an increase of activity over 100 h to 980 mol(H_2)/(mol(Pt)×h) and CO_2-selectivity of 99.4%. To investigate potential reactive transformations of the material under catalytic conditions further, the maximum temperature was increased to 400 °C in second test (Figure 3b). This leads to a strongly enhanced, but fluctuating activity between 3000 – 8000 mol(H_2)/(mol(Pt)×h) and a decrease of the CO_2-selectivity to 94 – 96% at 400 °C. This observation indicated fast material changes related to the applied gas-phase composition, as observed for copper in H_2 oxidation[36], leading to varying conversion. A more detailed investigation of this phenomenon is given in a later section of this paper. Additionally, the activity decreased by roughly 25% over 20 h at 400 °C. Heating the material in the feed first to 400 °C and subsequent catalysis at 300 °C results in a strong activity increase (1500 mol(H_2)/(mol(Pt)×h)) at an excellent selectivity of 99.5%.

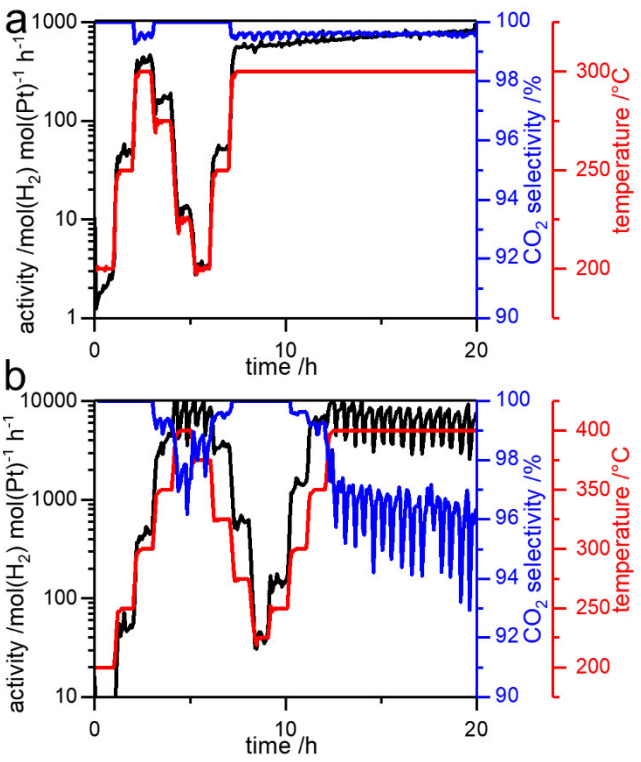

Figure 3: Catalytic tests of the pre-treated In_2Pt/In_2O_3 aerogel at 200 – 300 °C (a, 50 mg untreated material) and 200 – 400 °C (b, 25 mg untreated material). An unprecedented CO_2-selectivity of 99.5% is observed for both tests at 300 °C. In the test up

to 400 °C, an increase of activity at 300 °C can be observed after being heated to 400 °C. At 400 °C a strongly fluctuating catalytic behavior can be observed, for details refer to the text.

Comparison of this material with previously investigated materials (Figure 4) emphasizes the excellent performance, showing the highest observed selectivity and similar activity as ZnPd/ZnO aerogels.[37] It outperforms Cu-based materials[9,12,38], InPd/In_2O_3 materials[21,39], In-Pt-based materials[24] and other materials based upon intermetallic compounds[12,20,40,41] by an order of magnitude in activity and shows at least 50% less CO. The difference in activity at 300 °C with and without heat treatment at 400 °C indicates material changes upon heating and subsequent cooling that do not occur under prolonged time on stream at 300 °C.

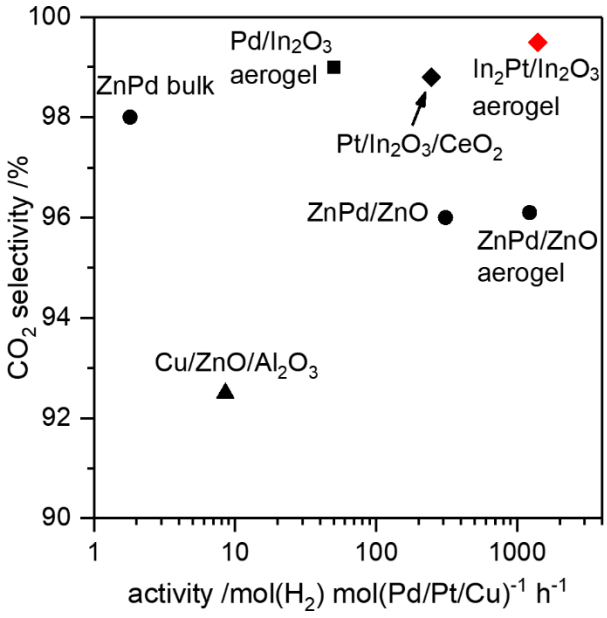

Figure 4: Comparison of the investigated In_2Pt/In_2O_3 aerogel with previously investigated materials[17,18,21,24,37,42] *at 300 °C.*

XRD analysis of the material after being subjected to MSR conditions (Figure 5) reveals a temperature-dependent stability of the pre-formed In_2Pt compound, in agreement with the indications from the pre-reduction. At 200 °C In_2Pt is stable under reaction conditions but partly decomposes at 300 °C into In_3Pt_2 due to the oxidation potential of the reactant stream. At 400 °C In_2Pt is formed again under reaction conditions due to the temperature dependence of the phase stability, emphasizing the dynamic temperature- and atmosphere-dependent redox-chemistry of the In-Pt system.

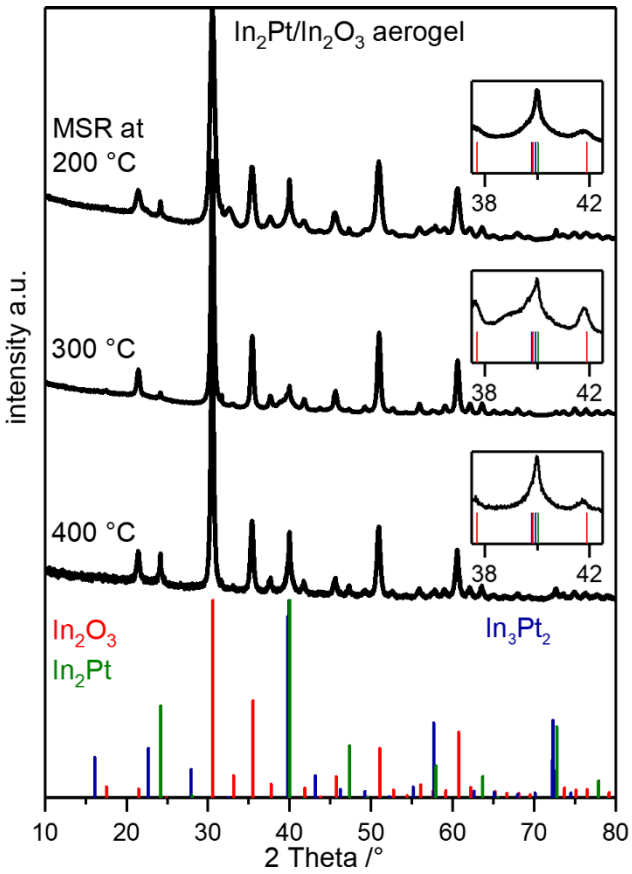

Figure 5: XRD patterns of the In_2Pt/In_2O_3 aerogel after being subjected to MSR conditions at 200 °C, 300 °C and 400 °C. Additionally shown are the calculated patterns of In_2O_3[33], In_2Pt[34] and In_3Pt_2.[34]

HR-TEM analysis of the material after catalytic operation at 400 °C as maximum temperature and subsequent operation at 300 °C reveals an amorphous layer on the Pt-containing particles and contrast inhomogeneities in HR-STEM (Figure 6). By EDX analysis (Figure 6c) it was identified that the amorphous layer is Pt-depleted and that the contrast inhomogeneities are caused by a lower amount of Pt in the particle core. Contrary to these findings, no changes in the elemental distribution or the surface region of the Pt-containing particles were identified on samples taken after being subjected to MSR conditions directly at 300 °C (Figure S8 and S9) or 400 °C (Figure S10). Thus, in the activated state at 300 °C, a high interface concentration between InO_x and In-Pt intermetallic compounds is present, caused by the thin layer of amorphous InO_x on the intermetallic particles. This layer formation apparently requires a decomposition of the initial In_2Pt particles and subsequent reactive transformation between In_2Pt and In_3Pt_2. Continuous decomposition and reformation of In_2Pt results in formation of In_2O_3 on top of the resulting In_3Pt_2 particles and incorporation of In_2O_3 from the support upon reduction. This does not occur if the In_2Pt particles remain stable, at 400 °C, or the reactive transformation is not pronounced enough, at 300 °C under isothermal conditions.

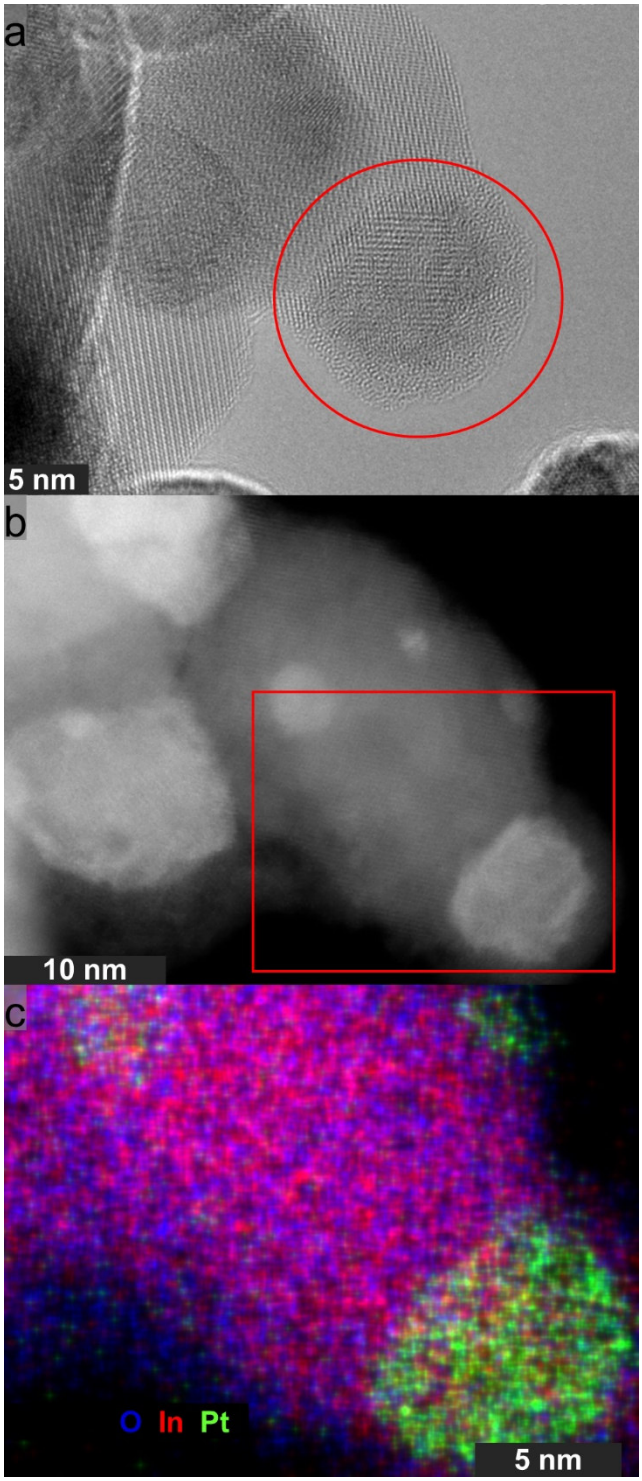

Figure 6: a) HR-TEM micrograph of an In_2Pt/In_2O_3 aerogel after being subjected to MSR conditions at 400 °C and subsequently cooled to 300 °C under MSR conditions. An amorphous layer covers the Pt-containing particles. b) HR-STEM micrograph of the material. The Pt-containing particles exhibit a lower Z-contrast in the core and exhibit a low contrast layer on the surface. c) EDX mapping of the area marked by the red rectangular in b). The layer is Pt-depleted, and the edges of the particle exhibit a higher Pt-content than the inner area.

Influence of the observed redox-activity on the catalytic cycle was investigated by sequential ^{18}O-labeled MSR at 300 °C (Figure 7). An initial unlabeled step (**I**) was conducted, to obtain a reference for the CO_2 formation. Subsequently, sequential switching to ^{18}O-labeled

(**II**) and back to unlabeled reactants (**III**) after thorough purging was utilized to investigate the role of chemically bound oxygen from the previous experimental phase in the catalytic cycle. Upon contact with ^{18}O-labeled reactants (**II**) the release of $C^{16}O_2$ is observed, followed by $C^{16}O^{18}O$ and $C^{18}O_2$. The high amount of the mixed CO_2 species might result from the formation of partly reduced In_2O_3. This can occur in the observed amorphous oxide layer and agrees with CO_2 hydrogenation over In_2O_3.[43] In the time frame of the isotope labelled experiment a complete exchange of all oxygen atoms in catalytic material is unlikely, due to the distribution of active sites and the calculated minimum time for a complete exchange (equations S1 and S2, table S1), allowing an overlap of catalytic and stoichiometric reactions during this experiment phase. In_2O_3 alone, i.e. without the intermetallic compounds cannot explain the observed activity (10 mmol(H_2)/(g(cat)×h)[21] vs. 600 mmol(H_2)/(g(cat)×h) for the In_2Pt/In_2O_3 material). Switching to unlabeled reactants (**III**) a short release of $C^{18}O_2$ and $C^{16}O^{18}O$ is observed. The timeframe is in the expectable region for the exchange oxygen from active InO_x species on the material. These experiments prove that oxygen from the reactants is incorporated into the material and subsequently released, suggesting a Mars-van-Krevelen mechanism. In comparison to a $InPd/In_2O_3$ aerogel[21], the In_2Pt/In_2O_3 shows faster kinetics in the release of the CO_2 species correlated to chemically bound oxygen, which reflects the overall higher activity of the material. Participation of chemically bound oxygen in MSR over Pt/In_2O_3 materials is in agreement with CO_2 hydrogenation investigations on Cu/Al_2O_3 materials[44] or pure In_2O_3.[43]

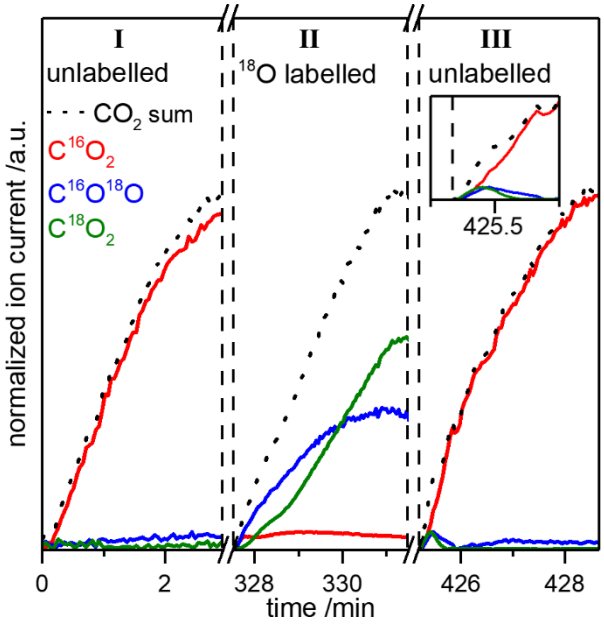

Figure 7: MS-signals for CO_2 with different oxygen isotopes during the initial contact of with the In_2Pt/In_2O_3 material (25 mg untreated material) and reactant stream. Experimental order was unlabeled reactants, ^{18}O-labeled reactants and unlabeled reactants after thoroughly purging with inert gas between every vapor composition. Dotted line represents the sum of the different CO_2 species.

The observed reactive transformation and the elemental distribution of Pt-containing particles as well as the participation of chemically bound oxygen by variation of the oxidation potential of the reactant stream at 400 °C leads to altered catalytic properties (Figure 8a). While a CH_3OH:H_2O ratio of 1:1 leads to the already shown highly fluctuating state (see also Figure 3), doubling of the water content leads to an increase of activity by 20% and a selectivity increase to 97.6%, compared to 96.6% as maximum value in the fluctuating state, and steady catalytic properties. In contrast, doubling of the methanol content leads to a decrease of activity by 50% and a selectivity decrease to 95.5% as maximum. The catalytic properties are not as steady as in the case of increased water content. XRD analysis (Figure 8b) reveals the presence of In_3Pt_2 and In_2Pt for the water-rich reactant stream, as for the 1:1 reactant feed at 300 °C, linked to the higher oxidation potential. Methanol content increase, which leads to a higher CO content, thus an increase of reduction potential, leads to the formation of In_7Pt_3 and elemental indium on the aerogel, hence limiting the synergistic effects between intermetallic compounds and indium oxide as well as the redox chemistry. Comparison of the results with the three different reactant ratios leads to the conclusion that the 1:1 ratio leads to the material switching it's chemical state to a more oxidized or reduced state between the border cases of the 1:2 and 2:1 ratio, respectively.

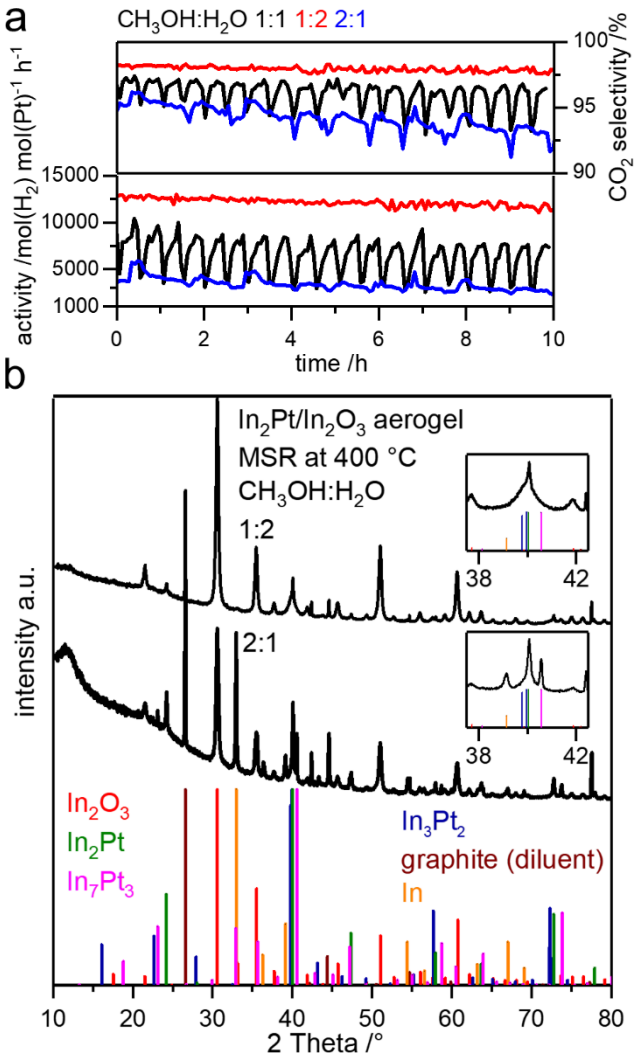

Figure 8: a) Isothermal MSR at 400 °C with varying $CH_3OH:H_2O$ ratio. b) XRD patterns of the material after being subjected to MSR at 400 °C with non-stoichiometrically reactant composition. Additionally shown are the calculated patterns of In_2O_3, In_2Pt, In_3Pt_2, In_7Pt_3, In[45] and graphite[46], which was used as diluent.

According to our findings (summarized in Scheme 1), In_2Pt is oxidized by water and forms In_3Pt_2 and In_2O_3. An amorphous layer consisting of InO_x grows on the In_3Pt_2 particles under reaction conditions. The defective In_2O_3 is then prone to (partial) reduction by reducing agents in the gas stream, e.g. CO, to form either oxygen vacancies, as observed in CO_2 hydrogenation[43], or re-form In_2Pt, which subsequently gets oxidized again. Excess of reducing agents like CO or CH_3OH leads to the formation of elemental indium and In_7Pt_3, resulting in lowered activity and selectivity. The oxidation of In_2Pt in this redox cycle can be prevented if either by high conversion, which leads to reducing conditions, or low water content in the reactant stream. Both result in a low oxidation potential of the gas phase, making an oxidation of In_2Pt unfavorable. This decreases the activity and selectivity of the material (Figure 3b), until the conversion becomes low enough to enable oxidation of In_2Pt again by an increase of the water content and decrease of the hydrogen content in the gas phase. This results in

fluctuating catalytic behavior, which can be circumvented by an increase of the water content in the reactants. The proposed redox cycle explains i) the high CO_2-selectivity by a CO removal step or enhancement of the MSR reaction path by partially reduced indium oxide species, enabling CO_2-selectivity above the limit of the WGS reaction by the dominant MSR reaction and ii) the strong change of the catalytic properties by adjustment of the material to the oxidation potential of the gas phase. Stoichiometric reactions of the catalytic material as origin of the high CO_2 selectivity can not explain the high selectivity over prolonged reaction time, since formation of reduced catalytically inactive InO_x species cannot occur for more than a few minutes, given the available oxygen reservoir in the material (table S1).

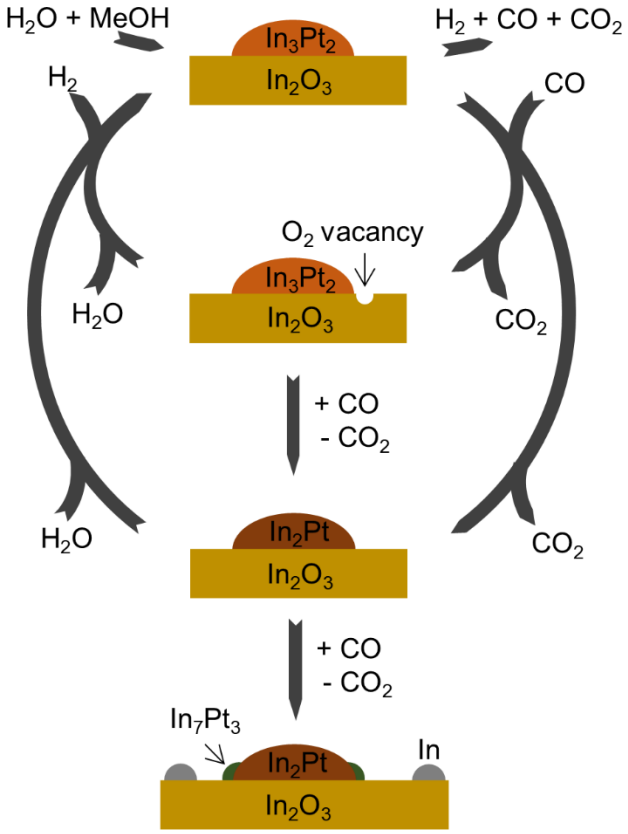

Scheme 1: Proposed redox cycle of an In_2Pt/In_2O_3 material under MSR conditions. Carbon monoxide or related intermediates act as reducing agents and form oxygen vacancies or reduce In_2O_3 in close proximity to In_3Pt_2. Formed In_2Pt subsequently undergoes oxidation by water, to re-form In_3Pt_2 and an In_2O_3 shell. Excess of reducing agents leads to the formation of In_7Pt_3 and indium.

Conclusions

In_2Pt/In_2O_3 aerogels were synthesized by a sol-gel approach and subsequent partial reduction obtained intermetallic compounds supported on a high specific surface area In_2O_3 support. Catalytic testing in MSR revealed very high activity and unprecedented CO_2-selectivity of 99.5% at 300 °C. Correlation of catalytic properties with identified phases by

XRD, nanoscopic changes by HR electron microscopy and ^{18}O-labeled MSR enabled the identification of redox-activity of In_2Pt and In_3Pt_2 with In_2O_3 under reaction conditions as cause of the excellent CO_2-selectivity, indicating a Mars-van-Krevelen mechanism. Adjustment of the gas phase oxidation potential allowed control of the reactive transformations of intermetallic compounds under reaction conditions and thus over the catalytic properties. The presence of amorphous oxide layers as center of redox activity appears to be a common concept in intermetallic MSR catalysts and is responsible for high activity as well as selectivity. Thus, controlling the formation and reactivity of these amorphous oxide layers to enable redox-activity of intermetallic compounds is crucial for further MSR catalyst developments.

Supporting Information

SEM and TEM micrographs of the as-prepared material, XRD pattern of the as prepared material, SEM and TEM micrographs of the pre-treated material, Arrhenius plot, isothermal catalytic test and additional HR-TEM micrographs after catalysis.

Acknowledgement

The Deutsche Bundesstiftung Umwelt is acknowledged for the financial support of the work of Lukas Thoni. Acknowledged is also the financial support, which has been received by the ERC AdG AEROCAT.

The authors thank Isabel Köwitsch and Prof. Michael Mehring, TU Chemnitz, Coordination Chemistry, for the XRD measurements.

References

(1) Asinger, F. *Methanol — Chemie- und Energierohstoff*, 1st ed.; Springer-Verlag: Berlin, Heidelberg, **1986**, 57-267. https://doi.org/10.1007/978-3-642-70763-6.

(2) Olah, G. A. Beyond Oil and Gas: The Methanol Economy. *Angew. Chemie Int. Ed.* **2005**, *44* (18), 2636–2639. https://doi.org/10.1002/anie.200462121.

(3) Goeppert, A.; Czaun, M.; Jones, J.-P.; Surya Prakash, G. K.; Olah, G. A. Recycling of carbon dioxide to methanol and derived products – closing the loop. *Chem. Soc. Rev.* **2014**, *43* (23), 7995–8048. https://doi.org/10.1039/C4CS00122B.

(4) Bertau, M.; Offermanns, H.; Plass, L.; Schmidt, F.; Wernicke, H. J. *Methanol: The Basic Chemical and Energy Feedstock of the Future*; Springer-Verlag: Berlin, Heidelberg, **2014**, 51-651. https://doi.org/10.1007/978-3-642-39709-7.

(5) Peppley, B. A.; Amphlett, J. C.; Kearns, L. M.; Mann, R. F. Methanol–steam reforming on $Cu/ZnO/Al_2O_3$ catalysts. Part 2. A comprehensive kinetic model. *Appl.*

Catal. A Gen. **1999**, *179* (1–2), 31–49. https://doi.org/10.1016/S0926-860X(98)00299-3.

(6) Shen, J. Influence of preparation method on performance of Cu/Zn-based catalysts for low-temperature steam reforming and oxidative steam reforming of methanol for H_2 production for fuel cells. *Catal. Today* **2002**, *77* (1–2), 89–98. https://doi.org/10.1016/S0920-5861(02)00235-3.

(7) Agrell, J. Production of hydrogen from methanol over Cu/ZnO catalysts promoted by ZrO_2 and Al_2O_3. *J. Catal.* **2003**, *219* (2), 389–403. https://doi.org/10.1016/S0021-9517(03)00221-5.

(8) Lucarelli, C.; Molinari, C.; Faure, R.; Fornasari, G.; Gary, D.; Schiaroli, N.; Vaccari, A. Novel Cu-Zn-Al catalysts obtained from hydrotalcite-type precursors for middle-temperature water-gas shift applications. *Appl. Clay Sci.* **2018**, *155*, 103–110. https://doi.org/10.1016/J.CLAY.2017.12.022.

(9) Sanches, S. G.; Flores, J. H.; da Silva, M. I. P. Cu/ZnO and Cu/ZnO/ZrO_2 catalysts used for methanol steam reforming. *Mol. Catal.* **2018**, *454*, 55–62. https://doi.org/10.1016/J.MCAT.2018.05.012.

(10) Águila, G.; Jiménez, J.; Guerrero, S.; Gracia, F.; Chornik, B.; Quinteros, S.; Araya, P. A novel method for preparing high surface area copper zirconia catalysts. Influence of the preparation variables. *Appl. Catal. A Gen.* **2009**, *360* (1), 98–105. https://doi.org/10.1016/j.apcata.2009.03.014.

(11) Oetjen, H.-F.; Schmidt, V. M.; Stimming, U.; Trila, F. Performance Data of a Proton Exchange Membrane Fuel Cell Using H_2/CO as Fuel Gas. *J. Electrochem. Soc.* **1996**, *143* (12), 3838–3842. https://doi.org/10.1149/1.1837305.

(12) Sá, S.; Silva, H.; Brandão, L.; Sousa, J. M.; Mendes, A. Catalysts for methanol steam reforming—A review. *Appl. Catal. B Environ.* **2010**, *99* (1–2), 43–57. https://doi.org/10.1016/j.apcatb.2010.06.015.

(13) Iwasa, N.; Mayanagi, T.; Ogawa, N.; Sakata, K.; Takezawa, N. New catalytic functions of Pd-Zn, Pd-Ga, Pd-In, Pt-Zn, Pt-Ga and Pt-In alloys in the conversions of methanol. *Catal. Letters* **1998**, *54* (3), 119–123. https://doi.org/10.1023/A:1019056728333.

(14) Iwasa, N.; Masuda, S.; Ogawa, N.; Takezawa, N. Steam reforming of methanol over

Pd/ZnO: Effect of the formation of PdZn alloys upon the reaction. *Appl. Catal. A Gen.* **1995**, *125* (1), 145–157. https://doi.org/10.1016/0926-860X(95)00004-6.

(15) Iwasa, N.; Takezawa, N. New supported Pd and Pt alloy catalysts for steam reforming and dehydrogenation of methanol. *Top. Catal.* **2003**, *22* (3–4), 215–224. https://doi.org/10.1023/A:1023571819211.

(16) Tsai, A. P.; Kameoka, S.; Ishii, Y. PdZn = Cu: Can an Intermetallic Compound Replace an Element? *J. Phys. Soc. Japan* **2004**, *73* (12), 3270–3273. https://doi.org/10.1143/JPSJ.73.3270.

(17) Friedrich, M.; Teschner, D.; Knop-Gericke, A.; Armbrüster, M. Influence of bulk composition of the intermetallic compound ZnPd on surface composition and methanol steam reforming properties. *J. Catal.* **2012**, *285* (1), 41–47. https://doi.org/10.1016/j.jcat.2011.09.013.

(18) Friedrich, M.; Penner, S.; Heggen, M.; Armbrüster, M. High CO_2 Selectivity in Methanol Steam Reforming through ZnPd/ZnO Teamwork. *Angew. Chemie Int. Ed.* **2013**, *52* (16), 4389–4392. https://doi.org/10.1002/anie.201209587.

(19) Heggen, M.; Penner, S.; Friedrich, M.; Dunin-Borkowski, R. E.; Armbrüster, M. Formation of ZnO Patches on ZnPd/ZnO during Methanol Steam Reforming: A Strong Metal-Support Interaction Effect? *J. Phys. Chem. C* **2016**, *120* (19), 10460–10465. https://doi.org/10.1021/acs.jpcc.6b02562.

(20) Lorenz, H.; Rameshan, C.; Bielz, T.; Memmel, N.; Stadlmayr, W.; Mayr, L.; Zhao, Q.; Soisuwan, S.; Klötzer, B.; Penner, S. From Oxide-Supported Palladium to Intermetallic Palladium Phases: Consequences for Methanol Steam Reforming. *ChemCatChem* **2013**, *5* (6), 1273–1285. https://doi.org/10.1002/cctc.201200712.

(21) Köwitsch, N.; Thoni, L.; Klemmed, B.; Benad, A.; Paciok, P.; Heggen, M.; Köwitsch, I.; Mehring, M.; Eychmüller, A.; Armbrüster, M. Proving a Paradigm in Methanol Steam Reforming: Catalytically Highly Selective In_xPd_y/In_2O_3 Interfaces. *ACS Catal.* **2021**, *11* (1), 304–312. https://doi.org/https://doi.org/10.1021/acscatal.0c04073.

(22) Kolb, G.; Keller, S.; Pecov, S.; Pennemann, H.; R., Z. Development of Micro-structured Catalytic Wall Reactors for Hydrogen Production by Methanol Steam Reforming over Novel $Pt/In_2O_3/Al_2O_3$ Catalysts. *Chem. Eng. Trans.* **2011**, *24*, 133–138. https://doi.org/10.3303/CET1124023.

(23) Liu, D.; Men, Y.; Wang, J.; Kolb, G.; Liu, X.; Wang, Y.; Sun, Q. Highly active and durable $Pt/In_2O_3/Al_2O_3$ catalysts in methanol steam reforming. *Int. J. Hydrogen Energy* **2016**, *41* (47), 21990–21999. https://doi.org/10.1016/j.ijhydene.2016.08.184.

(24) Liu, X.; Men, Y.; Wang, J.; He, R.; Wang, Y. Remarkable support effect on the reactivity of $Pt/In_2O_3/MO_x$ catalysts for methanol steam reforming. *J. Power Sources* **2017**, *364*, 341–350. https://doi.org/10.1016/J.JPOWSOUR.2017.08.043.

(25) Wang, Q.; Zhao, Z. L.; Zhang, Z.; Feng, T.; Zhong, R.; Xu, H.; Pantelides, S. T.; Gu, M. Sub-3 nm Intermetallic Ordered Pt_3In Clusters for Oxygen Reduction Reaction. *Adv. Sci.* **2019**, 1901279. https://doi.org/10.1002/advs.201901279.

(26) Jana, R.; Peter, S. C. One-pot solvothermal synthesis of ordered intermetallic Pt_2In_3 as stable and efficient electrocatalyst towards direct alcohol fuel cell application. *J. Solid State Chem.* **2016**, *242*, 133–139. https://doi.org/10.1016/J.JSSC.2016.02.016.

(27) Ramachandran, R. K.; Dendooven, J.; Filez, M.; Galvita, V. V; Poelman, H.; Solano, E.; Minjauw, M. M.; Devloo-Casier, K.; Fonda, E.; Hermida-Merino, D.; et al. Atomic Layer Deposition Route to Tailor Nanoalloys of Noble and Non-noble Metals. *ACS Nano* **2016**, *10* (9), 8770–8777. https://doi.org/10.1021/acsnano.6b04464.

(28) Wang, X.; Yang, D.; Xu, Y.; Zhong, J.; Zhang, Q. Colloidal Synthesis of Pt–In Bimetallic Nanoparticles for Propane Dehydrogenation. *Can. J. Chem.* **2017**, *95* (11), 1135–1140. https://doi.org/10.1139/cjc-2017-0033.

(29) Barbosa, R. L.; Papaefthimiou, V.; Law, Y. T.; Teschner, D.; Hävecker, M.; Knop-Gericke, A.; Zapf, R.; Kolb, G.; Schlögl, R.; Zafeiratos, S. Methanol Steam Reforming over Indium-Promoted Pt/Al_2O_3 Catalyst: Nature of the Active Surface. *J. Phys. Chem. C* **2013**, *117* (12), 6143–6150. https://doi.org/10.1021/jp309401q.

(30) Gash, A. E.; Tillotson, T. M.; Satcher, J. H.; Hrubesh, L. W.; Simpson, R. L. New sol-gel synthetic route to transition and main-group metal oxide aerogels using inorganic salt precursors. *J. Non. Cryst. Solids* **2001**, *285* (1–3), 22–28. https://doi.org/10.1016/S0022-3093(01)00427-6.

(31) Barthel, J.; Thust, A.; Tillmann, K. FEI Titan 80-300 TEM. *J. large-scale Res. Facil.* **2016**, *2* (A41), 1–4. https://doi.org/http://dx.doi.org/10.17815/jlsrf-2-66.

(32) Heggen, M.; Luysberg, M.; Tillmann, K. FEI Titan 80-300 STEM. *J. large-scale Res. Facil.* **2016**, *2* (A42), 1–3. https://doi.org/http://dx.doi.org/10.17815/jlsrf-2-67.

(33) Ambrosini, A.; Duarte, A.; Poeppelmeier, K. R.; Lane, M.; Kannewurf, C. R.; Mason, T. O. Electrical, Optical, and Structural Properties of Tin-Doped In_2O_3-M_2O_3 Solid Solutions (M = Y, Sc). *J. Solid State Chem.* **2000**, *153*, 41–47. https://doi.org/10.1006/jssc.2000.8737.

(34) Lin, C. F.; Mohney, S. E.; Chang, Y. A. Phase equilibria in the Pt-In-P system. *J. Appl. Phys.* **1993**, *74* (4398). https://doi.org/10.1063/1.354410.

(35) Friedrich, H. A.; Köhler, J. Refinement of the crystal structure of triplatinum heptaindium, Pt_3In_7. *Zeitschrift für Krist. - New Cryst. Struct.* **2002**, *217*, 24. https://doi.org/https://doi.org/10.1524/ncrs.2002.217.1.24.

(36) Cao, J.; Rinaldi, A.; Plodinec, M.; Huang, X.; Willinger, E.; Hammud, A.; Hieke, S.; Beeg, S.; Gregoratti, L.; Colbea, C.; et al. In situ observation of oscillatory redox dynamics of copper. *Nat. Commun.* **2020**, *11* (1), 1–11. https://doi.org/10.1038/s41467-020-17346-7.

(37) Ziegler, C.; Klosz, S.; Borchardt, L.; Oschatz, M.; Kaskel, S.; Friedrich, M.; Kriegel, R.; Keilhauer, T.; Armbrüster, M.; Eychmüller, A. ZnPd/ZnO Aerogels as Potential Catalytic Materials. *Adv. Funct. Mater.* **2016**, *26* (7), 1014–1020. https://doi.org/10.1002/adfm.201503000.

(38) Li, H.; Tian, H.; Chen, S.; Sun, Z.; Liu, T.; Liu, R.; Assabumrungrat, S.; Saupsor, J.; Mu, R.; Pei, C.; et al. Sorption enhanced steam reforming of methanol for high-purity hydrogen production over Cu-MgO/Al_2O_3 bifunctional catalysts. *Appl. Catal. B Environ.* **2020**, *276*, 119052. https://doi.org/10.1016/j.apcatb.2020.119052.

(39) Rameshan, C.; Lorenz, H.; Armbrüster, M.; Kasatkin, I.; Klötzer, B.; Götsch, T.; Ploner, K.; Penner, S. Impregnated and Co-precipitated Pd–Ga_2O_3, Pd–In_2O_3 and Pd–Ga_2O_3–In_2O_3 Catalysts: Influence of the Microstructure on the CO_2 Selectivity in Methanol Steam Re. *Catal. Letters* **2018**, *148* (10), 3062–3071. https://doi.org/10.1007/s10562-018-2491-4.

(40) Nowicka, E.; Althahban, S. M.; Luo, Y.; Kriegel, R.; Shaw, G.; Morgan, D. J.; He, Q.; Watanabe, M.; Armbrüster, M.; Kiely, C. J.; et al. Highly Selective PdZn/ZnO Catalysts for the Methanol Steam Reforming Reaction. *Catal. Sci. Technol.* **2018**, *8* (22), 5848–5857. https://doi.org/10.1039/C8CY01100A.

(41) Yan, P.; Tian, P.; Cai, C.; Zhou, S.; Yu, X.; Zhao, S.; Tu, S. T.; Deng, C.; Sun, Y.

Antioxidative and stable PdZn/ZnO/Al_2O_3 catalyst coatings concerning methanol steam reforming for fuel cell-powered vehicles. *Appl. Energy* **2020**, *268*, 115043. https://doi.org/10.1016/j.apenergy.2020.115043.

(42) Neumann, M.; Teschner, D.; Knop-Gericke, A.; Reschetilowski, W.; Armbrüster, M. Controlled synthesis and catalytic properties of supported In-Pd intermetallic compounds. *J. Catal.* **2016**, *340*, 49–59. https://doi.org/10.1016/j.jcat.2016.05.006.

(43) Tsoukalou, A.; Abdala, P. M.; Stoian, D.; Huang, X.; Willinger, M.-G.; Fedorov, A.; Müller, C. R. Structural Evolution and Dynamics of an In_2O_3 Catalyst for CO_2 Hydrogenation to Methanol: An Operando XAS-XRD and In Situ TEM Study. *J. Am. Chem. Soc.* **2019**, *141*, 13497–13505. https://doi.org/10.1021/jacs.9b04873.

(44) Lam, E.; Corral-Pérez, J. J.; Larmier, K.; Noh, G.; Wolf, P.; Comas-Vives, A.; Urakawa, A.; Copéret, C. CO_2 Hydrogenation on Cu/Al_2O_3: Role of the Metal/Support Interface in Driving Activity and Selectivity of a Bifunctional Catalyst. *Angew. Chemie - Int. Ed.* **2019**, *58* (39), 13989–13996. https://doi.org/10.1002/anie.201908060.

(45) Wu, Z.; Wegener, E. C.; Tseng, H.-T.; Gallagher, J. R.; Harris, J. W.; Diaz, R. E.; Ren, Y.; Ribeiro, F. H.; Miller, J. T. Pd–In intermetallic alloy nanoparticles: highly selective ethane dehydrogenation catalysts. *Catal. Sci. Technol.* **2016**, *6* (18), 6965–6976. https://doi.org/10.1039/C6CY00491A.

(46) He, J. L.; Shen, Z. Q.; Wu, E.; Liu, Z. Y.; He, L. L.; Yu, D. L.; Guo, L. C.; Wu, Q. H.; Luo, X. G.; Hu, Q. K.; et al. Carbon-rich boron carbide in the eutectic product synthesized by resistance heating of B_2CN in graphite. *J. Alloys Compd.* **2007**, *437* (1–2), 238–246. https://doi.org/10.1016/j.jallcom.2006.07.097.

For Table of Contents Only: ***Reactive transformation of In_2Pt and In_3Pt_2*** *in methanol steam reforming. Redox activity of intermetallic compounds and formation of a partly crystalline In_2O_3 layer are identified as cause for unprecedented CO_2-selectivity.*